Journal of Applied Mechanics and Technical Physics, Vol. 39, No. 1, 1998

NUMERICAL STUDIES OF TRANSPORTATION OF GRANULAR MATERIAL BY A PIN-POINT BLAST USING MODELS OF THE MECHANICS OF CONTINUOUS AND GRANULAR MEDIA

V. V. Borovikov

UDC 532.222.2

Mathematical models for numerical studies of transportation of a mass of loose granular material during occurrence of a series of deep gas-dynamic ejections are developed using methods of the mechanics of continuous and granular media. Features of the kinematics and dynamics of development of this phenomenon are analyzed. Results of a numerical experiment and recommendations on use of the models in studies of specific transportation regimes are given.

In the present paper, we study a phenomenon that is physically close to a pin-point ejection blast, which is used in blasting technologies. But, instead of chemical explosives, compressed gas is the energy source in this case. Pulsed feeding of compressed gas produces disintegration of an arbitrary discontinuity of parameters, and this can be classified as a physical explosion.

The principle of the transportation method consists in successive occurrence of a series of gas-dynamic ejections from deep sources that operate in the regime of a traveling wave. Transportation occurs as follows. A poured layer of granular material 1 (Fig. 1a) is placed on a transport tray 2. Sources of gas energy 3 are equally spaced at the bottom of the tray. Operation of the ith source produces a symmetric cavity A in the mass. Next, after a delay the $(i+1)$th source operates. As a result, an asymmetric cavity B forms, and the mass of granular material located between the cavities acquires a velocity in the direction of the line of least resistance OC, i.e., in the direction of transportation. Then the $(i+2)$th source comes into action, etc. The mass moves in a direction opposite to the direction of successive operation of the sources.

Transportation is also possible when camouflet cavities are produced in the mass (Fig. 1b). Thus, operation of the ith source produces a symmetric cavity A in the mass. Then, after a delay, during which the camouflet cavity A reaches maximum dimensions, the $(i+1)$th source operates. As a result a cavity B develops, and the mass of loose material moves in the direction of transportation, filling the cavity A.

The main factors governing the development of the process include the energy and flow rate of the gas per pulse, the delay of operation of the next source, the distance between the sources, the height of the layer, and the physical properties of the transported material.

Deep insight into the physical essence of the phenomenon can be gained from analysis of the correlation among the basic parameters (pressure, densities, velocities of both phases, stress state, packing, and porosity of the mass). Obviously, the transportation rate is largely determined by the pressure fields in the carrier phase and the stresses in the mass. Simultaneous control of the set of parameters can be successfully performed by mathematical modeling. In turn, the development of correct mathematical models requires information on the physical essence of the phenomenon. In this connection, we note that a feature of the process is repeated action on the mass by deep gas sources. As a result, the cohesion between grains is broken, and the medium can be regarded as cohesionless or loose. Under such conditions, the dry-friction forces in relative motion of the particles are large compared to the cohesive forces, which is typical of a loose medium. In mathematical

Mozhaisk Military Space-Engineering Academy, St. Petersburg 197082. Translated from Prikladnaya Mekhanika i Tekhnicheskaya Fizika, Vol. 39, No. 1, pp. 3–14, January–February, 1998. Original article submitted February 5, 1996; revision submitted June 19, 1996.

0021-8944/98/3901-0001 $20.00

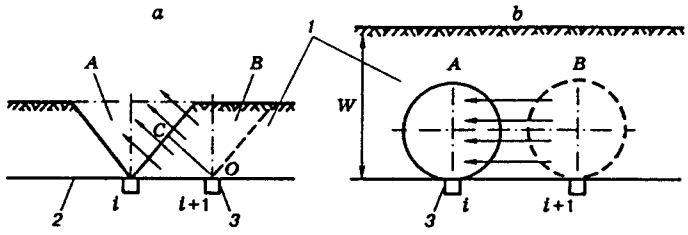

Fig. 1

modeling of multiphase flows, such a medium can be modeled using methods of the mechanics of disperse media (as a conglomerate of individual particles) or a phenomenological approach in which the mass of loose material is described by a continuous model. In the present work, both approaches are considered.

1. The model constructed using methods of the mechanics of continuous media [1] uses the following assumptions: the size of inhomogeneities (grains) in the mixture is much larger than the molecular-kinetic sizes; the size of inhomogeneities is much smaller than the distances at which the macroscopic parameters change significantly; the kinetic energy of small-scale motion of the carrier phase can be ignored; the average tensor of viscous stresses for the carrier phase is small (the viscosity of the gas will be taken into account only in the interphase interaction force); there are no phase transitions; the mixture is monodisperse (the grains of the loose material are of equal size); random motion of particles can be ignored; there is no comminution or coalescence of solid undeformable particles; displacements of the disperse phase and variations in its true density are significant.

As the basis for the mathematical model, it is expedient to use the approach adopted in [1], where the interpenetrating motion of the carrier phase and the disperse phase is described by a heterogeneous model of two continuous media. According to the adopted assumptions, the equations of conservation of mass and momentum of the phases are written in two-dimensional form as

$$\frac{\partial \rho_1}{\partial t} + \nabla^k \rho_1 \mathbf{V}_1^k = 0; \tag{1.1}$$

$$\frac{\partial \rho_2}{\partial t} + \nabla^k \rho_2 \mathbf{V}_2^k = 0; \tag{1.2}$$

$$\rho_1 \frac{d_1 \mathbf{V}_1}{dt} = -\nabla \alpha_1 P_1 - \mathbf{R}_{12} + \rho_1 \mathbf{g}; \tag{1.3}$$

$$\rho_2 \frac{d_2 \mathbf{V}_2}{dt} = -\nabla \alpha_2 P_1 + \nabla^k \sigma_f^k + \mathbf{R}_{12} + \rho_2 \mathbf{g}. \tag{1.4}$$

Here ρ_1 and ρ_2 are the densities of the carrier and disperse phases, respectively, $\mathbf{V}_1^k$ and $\mathbf{V}_2^k$ are the velocity components of the carrier and disperse phases in the direction of the coordinate k, ∇ is a differential operator, α_1 and α_2 are the concentrations of the carrier and disperse phases, respectively, $\rho_1 \mathbf{g}$ and $\rho_2 \mathbf{g}$ are the mass-force vectors; P_1 is the pressure in the carrier phase, σ_f^k is the effective (contact) stress in the skeleton of the disperse phase, and $\mathbf{R}_{12}$ is the interphase force, which is generally expressed as $\mathbf{R}_{12} = -P_1 \nabla \alpha_1 - \mathbf{F}_\mu - \mathbf{F}_m$, where the quantity $\mathbf{F}_\mu$ is due to viscous forces at the phase interface (the viscous-friction force) and $\mathbf{F}_m$ is associated with small-scale pressure fluctuations due to acceleration of the phases relative to each other (the added-mass force):

$$\mathbf{F}_m = \chi_m \rho_1^0 \alpha_1 \alpha_2 \left(\frac{d\mathbf{V}_1}{dt} - \frac{d\mathbf{V}_2}{dt} \right). \tag{1.5}$$

Here $\rho_1^0 = \rho_1 / \alpha_1$ is the true density of the solid phase and χ_m is the added-mass coefficient. For a monodisperse mixture with spherical particles of radius a at concentrations lower than the packing density, we have $\chi_m = 0.5$.

The substantive derivatives associated with the motion of the ith component are defined by the relation

$$\frac{d_i}{dt} = \frac{\partial}{\partial t} + V_i^k \frac{\partial}{\partial x^k}.$$

The viscous-friction force for relative motion of the phases is determined using the friction coefficient C_μ. The empirical relations obtained for stationary blowing of gases through a poured layer of a loose medium of different porosity [2] are of the form

$$C_\mu = C_\mu^{(1)} = \frac{24}{\mathrm{Re}_{12}} + \frac{4.4}{\mathrm{Re}_{12}^{0.5}} + 0.42, \quad \alpha_2 \leqslant 0.08; \tag{1.6}$$

$$C_\mu = \frac{(\alpha_2 - 0.08)C_\mu^{(2)} + (0.45 - \alpha_2)C_\mu^{(1)}}{0.37}, \quad 0.08 < \alpha_2 \leqslant 0.45; \tag{1.7}$$

$$C_\mu = C_\mu^{(2)} = \frac{4}{3\alpha_1}\left(1.75 + \frac{150\alpha_2}{\alpha_1 \mathrm{Re}_{12}}\right), \quad 0.45 \leqslant \alpha_2. \tag{1.8}$$

The Reynolds number used in (1.6)–(1.8) is determined from the formula $\mathrm{Re}_{12} = (2a\rho_1^0\omega_{12})/\mu_1$, where ω_{12} is the relative velocity of motion of the phases and μ_1 is the dynamic viscosity of the gas (for air, $\mu_1 = 1.7 \cdot 10^{-5}$ Pa·sec). However, since interphase interaction also occurs at high concentrations of the disperse phase, the interaction forces should reflect constraints on the relative motion of the phases. In this connection, the Reynolds number must be represented with allowance for the ratio of the phase concentrations:

$$\mathrm{Re}_{12*} = \frac{\alpha_1 \mathrm{Re}_{12}}{\alpha_{1*}} = \frac{\alpha_1 \mathrm{Re}_{12}}{1 - b\alpha_2^{2/3}}. \tag{1.9}$$

Here $b \approx 1.16$ [2].

Generally, the viscous-friction force is

$$\mathbf{F}_\mu = C_\mu \pi a^2 \frac{\rho_1^0 \omega_{12}^2}{2}. \tag{1.10}$$

According to the last assumption that the model must take into account significant displacements of the disperse phase, the momentum equations (1.3) and (1.4) with allowance for (1.5) and (1.10) are written as

$$\rho_1(1 + \chi_m\alpha_2)\frac{d_1\mathbf{V}_1}{dt} - \chi_m\alpha_2\rho_1\frac{d_2\mathbf{V}_2}{dt} = -\alpha_1\nabla P_1 - \mathbf{F}_\mu + \rho_1\mathbf{g},$$

$$-\chi_m\alpha_2\rho_1\frac{d_1\mathbf{V}_1}{dt} + (\rho_2 + \chi_m\alpha_2\rho_1)\frac{d_2\mathbf{V}_2}{dt} = -\alpha_2\nabla P_1 + \frac{\partial\sigma_f^k}{\partial x^k} + \mathbf{F}_\mu + \rho_2\mathbf{g}.$$

Reducing these expressions to a form that is convenient for numerical calculations, we obtain

$$\frac{d_1\mathbf{V}_1}{dt}[\rho_2 + \chi_m\alpha_2(\rho_1 + \rho_2)] = -\nabla P_1\left(\chi_m\alpha_2^2 + \frac{\rho_2\alpha_1}{\rho_1} + \chi_m\alpha_1\alpha_2\right)$$
$$+ \frac{\partial\sigma_f^k}{\partial x^k}\chi_m\alpha_2 - \mathbf{F}_\mu\frac{\rho_2}{\rho_1} + \chi_m\alpha_2(\rho_1\mathbf{g} + \rho_2\mathbf{g}) + \rho_2\mathbf{g}; \tag{1.11}$$

$$\frac{d_2\mathbf{V}_2}{dt}[\rho_2 + \chi_m\alpha_2(\rho_1 + \rho_2)] = -\nabla P_1\left(\chi_m\alpha_2^2 + \alpha_2 + \chi_m\alpha_1\alpha_2\right)$$
$$+ \left(\frac{\partial\sigma_f^k}{\partial x^k} + \rho_2\mathbf{g}\right)(1 + \chi_m\alpha_2) + \mathbf{F}_\mu + \chi_m\alpha_2\rho_1\mathbf{g}. \tag{1.12}$$

According to [3], in constructing a computational algorithm based on a model of unsteady gas-dynamic flow, it is expedient to use the method of large particles. This allows one to obtain divergent conservative or dissipative steady-state schemes and to reveal the properties of solutions, including those for limiting flow regimes. In this connection, it is necessary to reduce Eqs. (1.11) and (1.12) to divergent form. For this, Eqs. (1.1) and (1.2) should be multiplied by the velocities of the corresponding phases and added to (1.11) and

(1.12). As a result, the momentum equations take the form

$$\frac{\partial \rho_1 \mathbf{V}_1}{\partial t}+\frac{\partial \rho_1 \mathbf{V}_1^2}{\partial x}=-\nabla P_1\frac{\chi_m\alpha_2\rho_1+\rho_2\alpha_1}{\chi_m\alpha_2(\rho_1+\rho_2)+\rho_2}+\left[\frac{\partial \sigma_f^k}{\partial x^k}-\frac{\rho_2}{\chi_m\alpha_2}\left(\frac{\mathbf{F}_\mu}{\rho_1}-\mathbf{g}\right)+(\rho_2+\rho_1)\mathbf{g}\right]\left[\frac{\rho_2}{\rho_1\chi_m\alpha_2}+\frac{\rho_2}{\rho_1}+1\right]; \quad (1.13)$$

$$\frac{\partial \rho_2 \mathbf{V}_2}{\partial t}+\frac{\partial \rho_2 \mathbf{V}_2^2}{\partial x}=-\nabla P_1\frac{\alpha_2\rho_2(\chi_m+1)}{\chi_m\alpha_2(\rho_1+\rho_2)+\rho_2}+\left[\left(\frac{\partial \sigma_f^k}{\partial x^k}+\mathbf{F}_\mu+\rho_2\mathbf{g}\right)\left(\frac{1}{\chi_m\alpha_2}+1\right)-\mathbf{F}_\mu+\rho_1\mathbf{g}\right]\left[\frac{1}{\chi_m\alpha_2}+1+\frac{\rho_1}{\rho_2}\right]. \quad (1.14)$$

To define the pressure in the carrier phase, it is necessary to use the equation of state

$$P_1=\rho_1^0 R T_1, \quad (1.15)$$

where T_1 is the gas temperature and R is the gas constant.

In the case where the carrier medium is a gas, the heat-flux equations are

$$\rho_1 c_1\frac{d_1 T_1}{dt}=\frac{\alpha_1 P_1}{\rho_1^0}\frac{d_1\rho_1^0}{dt}+\frac{\partial}{\partial x^k}\left(\lambda_1\frac{\partial T_1}{\partial x^k}\right)+Q_1+\mathbf{F}_\mu(\mathbf{V}_1-\mathbf{V}_2); \quad (1.16)$$

$$\rho_2 c_2\frac{d_2 T_2}{dt}=\frac{\partial}{\partial x^k}\left(\lambda_2\frac{\partial T_2}{\partial x^k}\right)+Q_2. \quad (1.17)$$

Here c_1 is the specific heat of the carrier phase at constant pressure, c_2 is the specific heat of the disperse phase, λ_1 and λ_2 are the thermal conductivities of the carrier and disperse phases, respectively, and Q_i is the rate of interphase heat exchange:

$$Q_1=S_{12}a_1^{-1}\lambda_1\mathrm{Nu}_1(T_s-T_1); \quad (1.18)$$

$$Q_2=S_{12}a_1^{-1}\lambda_1\mathrm{Nu}_2(T_s-T_2). \quad (1.19)$$

The quantity T_s is obtained from the condition $Q_1=-Q_2$ and characterizes the average temperature at the phase interface:

$$T_s=(\lambda_1\mathrm{Nu}_1T_1+\lambda_2\mathrm{Nu}_2T_2)/(\lambda_1\mathrm{Nu}_1+\lambda_2\mathrm{Nu}_2). \quad (1.20)$$

According to experimental studies [4], the Nusselt number as a characteristic of heat removal for a sphere is appropriate for use in the processes considered in the form

$$\mathrm{Nu}_1=2+0.459\,\mathrm{Re}_{12}^{0.55}\mathrm{Pr}_1^{0.33}, \quad \mathrm{Pr}_1=(c_1\mu_1)/\lambda_1, \quad (1.21)$$

where Pr_1 is the Prandtl number. Relation (1.21) is valid over a rather broad range of parameters: $1<\mathrm{Re}<70{,}000$ and $0.6<\mathrm{Pr}<400$.

According to [2], $\mathrm{Nu}_2\approx 10$ is used in formula (1.19) for the intensity of heat exchange between the surface of a disperse particle and the carrier phase.

In relations (1.18) and (1.19), the friction parameter a_1 is determined from known values of the concentration and permeability of the disperse phase and the Reynolds number [2, 5].

The parameter S_{12} characterizes the phase interface in a unit volume of the mixture:

$$S_{12}=(n4\pi a^2)/V_{\mathrm{calc}}, \quad n=(3V_{\mathrm{calc}}\alpha_2)/(4\pi a^2). \quad (1.22)$$

Here n is the number of particles of the solid phase in the volume of a cell of the calculation region V_{calc} (in Cartesian coordinates, $V_{\mathrm{calc}}=dx\cdot dy\cdot dz$).

Loading of the mass can be taken into account using a macroscopic theory that extends Hooke's law to a saturated porous medium. In this case, the tensor of effective stresses σ_f^{kl} is determined by Hooke's law through the tensor of effective stresses of the granular skeleton. The macrostrain tensor for the second phase is determined from the average displacements $[h_2^{kl}]$ of an elementary macrovolume:

$$\varepsilon_2^{kl}=0.5\left(\frac{\partial[h_2^l]}{\partial x^k}+\frac{\partial[h_2^k]}{\partial x^l}\right). \quad (1.23)$$

Then, the average tensor of effective stresses has the form

$$\sigma_f^{kl} = \alpha_2\Big[\lambda_f^{(s)}\varepsilon_2^{mm}\delta^{kl} + 2\mu_f^{(s)}\varepsilon_2^{kl} + \vartheta_f^{(s)}P_1\delta^{kl} - \vartheta_f^{(s)}\Big(\lambda_f^{(s)} + \frac{2\mu_f^{(s)}}{3}\Big)\beta_{T2}\Big(\frac{T_2}{T_0} - 1\Big)\delta^{kl}\Big], \tag{1.24}$$

where δ^{kl} is the Kronecker delta ($\delta^{kl} = 1$ for $k = l$ and $\delta^{kl} = 0$ for $k \neq l$), β_{T2} is the thermal-expansion coefficient of the material, and $\lambda_f^{(s)}$ and $\mu_f^{(s)}$ are the effective elastic moduli of the material.

The modulus $\vartheta_f^{(s)}$ characterizes the cohesion of the grains and determines the packing intensity of the mass under forced deformation. It is uniquely determined via the Lamé elastic moduli:

$$\vartheta_f^{(s)} = (\lambda^{(s)} + 2/3\mu^{(s)})/(\lambda_2^{(s)} + 2/3\mu_2^{(s)}). \tag{1.25}$$

The value of the modulus $\vartheta_f^{(s)} \ll 1$ corresponds to soft media, and for $\alpha_2\vartheta_f^{(s)} = 1$ the medium is ideally cemented.

The Lamé elastic moduli are expressed in terms of the strain modulus E and the Poisson ratio ϑ:

$$\lambda^{(s)} = E\vartheta/[(1+\vartheta)(1-2\vartheta)], \quad \mu^{(s)} = E/[2(1+\vartheta)]. \tag{1.26}$$

For grains of quartz sand, $E = 96.4$ GPa, and for a sand mass, $E \approx 1.2 \cdot 10^7$ Pa. The Poisson ratio is $\vartheta = 0.25$–0.3.

Equations (1.1), (1.2), (1.5)–(1.10), and (1.13)–(1.26) serve as a mathematical basis for the development of an algorithm for numerical simulation of a pin-point physical explosion in a mass of a loose medium. Because of the clearly expressed asymmetry of the phenomenon, it is expedient to construct the computational algorithm in two-dimensional Cartesian coordinates.

Previous experimental results [6] show that the process is most intense under initial conditions where a single gas-dynamic ejection in a mass produces a cavity with an insignificant blasting factor (the ratio of the cavity radius to the depth of location of the charge). In this connection, in the numerical experiment, the range of the initial conditions considered corresponds to this ejection regime.

The initial conditions include the physical properties and parameters of the gas phase (air) and the solid (quartz sand), the depth of the transported-material layer, the coordinates of the gas-energy sources along the axes, the distance between the sources, and the delay of operation of the $(i+1)$th source. To organize an algorithm by a first-order finite-difference scheme, a layer of fictitious cells is introduced at each edge of the calculation region.

The boundary conditions for the flow of the gas and solid phases in the lower portion of the calculation region (at the bottom of the transport tray) are specified as nonpenetration conditions. In the remaining parts of the boundaries, the gas phase has the possibility of free outflow. The solid phase above the level of the daytime surface W can also move freely beyond the calculation region. Below the level W at the right and left edges of the calculation region nonpenetration conditions were specified for the solid phase.

The dimensions of the calculation region, 80×50, ensured calculations with insignificant (about 2–3 %) disturbance of the mass balance of the solid phase due to outflow of it beyond the control space.

Results of the numerical simulation agree with results of experimental studies (by the criterion of transportation rate) with an accuracy of about 20%. In physical experiments, it is difficult to ensure continuous control of the simultaneously varying set of basic parameters. Numerical experiments are free of such a drawback.

Figure 2 illustrates the distribution of the velocity, stress, and density fields in the mass in the stage of operation of the ith gas source. In this stage, the process develops symmetrically. The intensity of each of the parameters is shown by isolines. As an illustration of the qualitative features of numerical calculation, Fig. 2 shows the transportation process under the following initial conditions: depth of the layer of loose material $W = 0.17$ m, distance between the sources $a = 0.15$ m, dimensions of the transport tray $1.0 \times 0.5 \times 0.02$ m, delay of operation of the $(i+1)$th source $t = 0.03$ sec, and gas pressure in the sources $P_z = 5 \cdot 10^5$ Pa (total energy of the gas with allowance for the degree of expansion $E_{\text{total}} = 40$ J).

The pattern of development of the phenomenon obtained by numerical simulation agrees with results

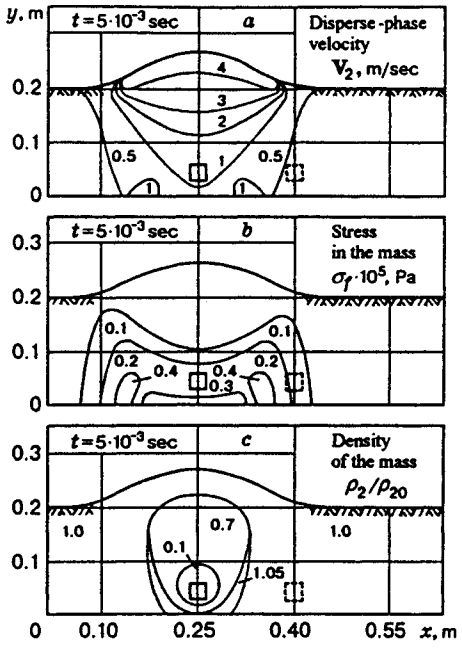

Fig. 2

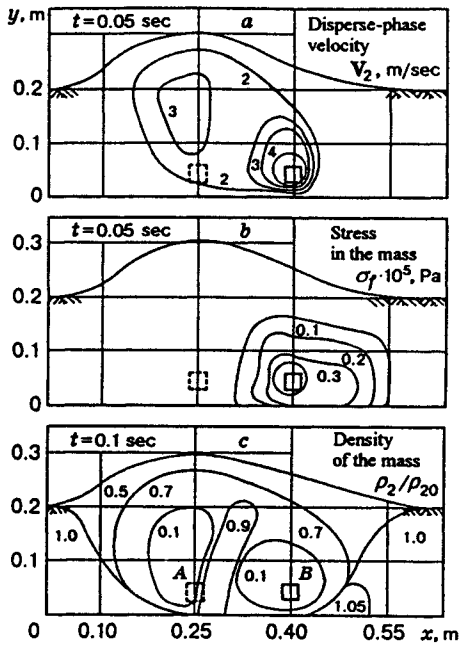

Fig. 3

of photorecording of the process in experiments. In particular, the largest value of the velocity of the mass is observed at the daytime-surface line. Figure 2a shows the beginning of formation of an ejection sheaf, which is an inverted cone with the apex at the center of the charge. The disperse phase is accelerated in the horizontal direction as well, but its velocity is markedly lower than in motion toward the free surface. This is caused by the counteraction of the effective stresses at points of particle contact (Fig. 2b) under compression of the mass. The stresses are significant in regions of the mass in which its displacement is limited. The largest stresses arise at the bottom of the transport tray and decrease with approach to the daytime surface. At the epicenter of the ejection, a rarefaction wave propagates from the daytime surface into the depth of the mass. This agrees with the data in Fig. 2a.

The evolution of the disperse phase is shown in Fig. 2c. At the real time $t = 5 \cdot 10^{-3}$ sec, the lowest density is observed at the center of the charge, indicating the beginning of formation of a camouflet cavity. The disperse-phase density near the center of the ejection changes continuously, decreasing with distance from the point of location of the energy source. Near the source, a certain increase in density (about 5–6%) relative to the initial density is observed outside the camouflet cavity. This indicates packing of individual particles of the loose material in denser aggregates. This property is most pronounced at the impenetrable wall of the transport tray.

The characteristic features of the development of the phenomenon upon operation of the $(i + 1)$th source are characterized foremost by asymmetry. In particular, the velocity of the mass is highest from the side of the camouflet cavity produced by the previous ejection (Fig. 3a). Therefore, the disperse phase located between the sources has a momentum whose vector points toward the transportation. This kinematics is due to both the pressure gradient in the carrier phase and the gradient of effective stresses. Zones of elevated stresses (Fig. 3b) are shown by isolines, which are shifted from the center of the $(i + 1)$th ejection toward the rigid bottom of the transport tray and toward the mass with the initial bulk density, undisturbed by the ith ejection. From the side of the cavity produced by the ith ejection, i.e., along the line of least resistance, the intensity of the stress fields is markedly lower.

The displacement of the disperse phase located between the sources is shown in Fig. 3c. Obviously, the development of the $(i + 1)$th ejection causes a less significant rise of the mass above the initial level of the daytime surface. This is compensated for by motion of the mass in the direction of transportation. As a result, cavity A is filled with unidirectionally moving disperse phase, and cavity B develops asymmetrically.

i.e., in the direction of transportation.

Numerical experiments permit extending the range of the parameters studied, which is sometimes unattainable in physical experiments. Thus, in a physical experiment, it was difficult to detect the variation of the parameters in the mass upon ejection from two sources with a small delay (about $2 \cdot 10^{-2}$ sec). This complicated the analysis of the physical essence of the phenomenon, which in this case was characterized by a certain decrease in the transportation index [6]. At the same time, numerical simulation of the phenomenon in this range of the parameters shows that early start of the next source causes counter motion of fragments of the mass in the zone between the sources. This is responsible for exchange of momentum, a decrease in the horizontal velocity, and an increase in the effective stresses on the boundary between the sources, which hinders displacement of the disperse phase in the direction of transportation.

2. The methods of the mechanics of loose media are based on representation of the transported mass as a conglomerate of individual particles. This approach is due to the course of the process, which is accompanied by repeated pulsed gas-dynamic action on the mass. Therefore, it is reasonable to assume that there is no cohesion or there is a small degree of cohesion between individual particles. This method of modeling can also take into account the mechanism of directed mass transport associated with collisions of particles during their evolution in space. Modeling of a mass of transported material by a conglomerate of discrete particles eliminates mathematical conditionalities in the description of discontinuities in the continuum of the dispersed phase during its evolution and gives clear insight into the location of the discontinuities in space.

In models of the mechanics of loose media, the particles have a definite shape and all the properties of solid bodies. The medium thus modeled resists external compressive loads and does not resist tensile loads. The evolution of its fragments is necessarily accompanied by a change in volume due to packing of the particles. The particles tend to form aggregates with a definite order of arrangement, depending on the shape of the particle surface. This causes a change in the volume of the pore space. The porosity is a factor that governs the development of the phenomenon. It can be described by the relation $\alpha_1 = 1 - \rho/\rho_2^0$, where ρ is the mass of a unit volume of the two-phase medium and ρ_2^0 is the true density of the solid phase of the mass. In experiments [6], α_1 varies from 0.15 to 0.42. In this connection, we examine the correctness of modeling the solid phase by individual spherical particles packed in aggregates.

Deresevich [7] performed a mathematical analysis of the types of packing of grains of a solid phase. The grains are treated as equal-sized, contacting spheres that are arranged in space in a regular order. Results of the analysis show that the porosity of a mass of such particles varies from 0.29 to 0.47, depending on the type of packing. Comparison of this index with the range of α_1 in experiments shows that the experimental range of α_1 agrees with data calculated for the packing of spherical particles in aggregates. This shows the possibility of representing a mass of transported material by a conglomerate of individual spherical particles.

In a mathematical description of the process, it is expedient to use a heterogeneous model that takes into account the interpenetrating motion of the two media in the presence of a relative velocity and a definite mechanism of their interaction. This model describes most adequately the motion of a medium with high porosity and low concentration of the solid phase, i.e., when the difference in velocity between the phases has a significant effect on the flow parameters. These parameters are largely determined by phase interaction forces. Excluding small-scale effects, the present model takes into account the aerodynamic, Archimedes, and added-mass forces.

The aerodynamic-drag force acting on an individual particle under restricted conditions of motion can be defined by (1.6)–(1.10).

The Archimedes force acting on a particle is determined by the pressure gradient in the carrier medium and the acceleration of the flow:

$$\mathbf{F}_{\text{Archimedes}} = \frac{4\pi a^3}{3} \rho_1^0 \left(\frac{d\mathbf{V}_1}{dt} - \mathbf{g}_1 \right). \tag{2.1}$$

Here $\mathbf{g}_1$ has the meaning of external mass forces.

The added-mass force $\mathbf{F}_m$ is determined by the inertial effects caused by particle motion in a dense

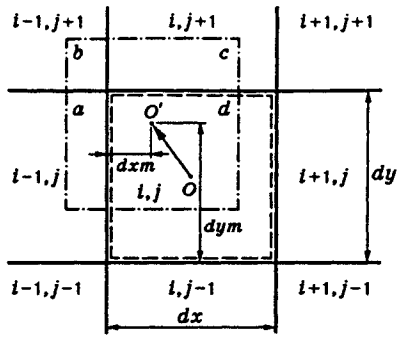

Fig. 4

medium. For motion of particles of constant size and shape in a gas, we have

$$\mathbf{F}_m = \chi_m \rho_1^0 \alpha_1 \alpha_2 \left(\frac{d\mathbf{V}_1}{dt} - \frac{d\mathbf{V}_2}{dt} \right), \tag{2.2}$$

where χ_m is the added-mass coefficient (for a sphere, $\chi_m = 0.5$).

The gravitational force acting on an individual particle can be written as $\mathbf{F}_G = \rho_2 \mathbf{g} W_2$, where W_2 is the volume of the solid phase within the calculation cell.

Thus, the equations of motion of a single particle in the absence of mass and heat exchange are written in vector form as

$$m \frac{\partial \mathbf{V}_2}{\partial t} = \mathbf{F}_\mu + \mathbf{F}_{\text{Archimedes}} + \mathbf{F}_m + \mathbf{F}_G,$$

where $\mathbf{V}_2$ is the velocity of the solid phase.

In the presence of shocks in the region of integration, the system of equations that describe the gas flow in two-dimensional Cartesian coordinates is conveniently written in the form of unsteady Euler equations:

$$\frac{\partial \rho_1}{\partial t} + \operatorname{div}(\rho_1 \mathbf{V}_1) = 0, \quad \frac{\partial \rho_1 v_1}{\partial t} + \operatorname{div}(\rho_1 v_1 \mathbf{V}_1) + \frac{\partial P_1}{\partial x} - \mathbf{F}_s = 0,$$

$$\frac{\partial \rho_1 u_1}{\partial t} + \operatorname{div}(\rho_1 u_1 \mathbf{V}_1) + \frac{\partial P_1}{\partial y} - \mathbf{F}_s = 0, \quad \frac{\partial \rho_1 E_1}{\partial t} + \operatorname{div}(\rho_1 E_1 \mathbf{V}_1) + \operatorname{div}(P_1 \mathbf{V}_1) = 0.$$

Here $\mathbf{F}_s$ is the overall vector of the forces (1.10), (2.1), and (2.2) that act on a unit mass of the disperse phase in the calculation cell.

For closure of this system, the following equation of state is used: $P_1 = P_1(\rho_1, I_1)$. The specific internal energy is expressed in terms of the total energy E_1 and the velocity: $I_1 = E_1 - \mathbf{V}_1^2/2$. Finally, we have $P_1 = (k-1)\rho_1(E_1 - \mathbf{V}_1^2/2)$.

A numerical algorithm for the gas flow was developed using the method of large particles. At the same time, the description of the evolution of the solid phase is based on the method of particles in cells. which is graphic, gives an analogy between calculation and experiment, and permits investigating complex phenomena in the dynamics of multicomponent flows. However, a characteristic feature of this method is computational instability. In the classical use of the method, the instability was suppressed by increasing the number of particles in one cell of an Eulerian grid. This smooths out the jumps in the parameters in the calculation region with passage of a particle from one cell to another. However, it has been shown that. despite the significant evolution of computer facilities, such a solution of the stability problem involves a considerable increase in computer time. Thus, taking into account that for modeling of collision processes, in each integration step exhaustive use of all particles by pairs is required, it is questionable whether constructing this model is appropriate.

In this connection, for solution of the posed problem, we employed the method of cellular-continuous representation of discrete particles of the solid phase. Figure 4 shows the mass-transfer process using this

method. At the beginning of the process there is mass M (one particle) of the disperse phase present in a calculation cell i, j. The local coordinates (within the cell) of the mass $0.5dx, 0.5dy$ correspond to the point O. The value of M is determined by the given porosity of the mass α_1, the volume of the cell V_{calc}, and the true density of the solid phase: $M = V_{\text{calc}}(1 - \alpha_1)\rho_2^0$. It is arbitrarily assumed that the mass of the particle is continuously located inside the cell and their boundaries coincide (Fig. 4, dashed lines).

Next, under the action of the carrier phase, the particle is displaced and occupies the local coordinates dxm, dym (point O′) within the cell i, j with dimensions dx, dy. Part of its mass is transferred to neighboring cells (Fig. 4, dot-and-dashed lines), and the new values of the mass in the cells are of the form

(a) $M_{(i-1,j)} = M_{(i-1,j)} + (dx/2 - dxm)(dy - dym + dy/2)\, dx\, \rho_2(1 - \alpha_1)$;
(b) $M_{(i-1,j+1)} = M_{(i-1,j+1)} + (dx/2 - dxm)(dym - dy/2)\, dx\, \rho_2(1 - \alpha_1)$;
(c) $M_{(i,j+1)} = M_{(i,j+1)} + (dx/2 + dxm)(dym - dy/2)\, dx\, \rho_2(1 - \alpha_1)$;
(d) $M_{(i,j)} = M_{(i,j)} + (dx/2 + dxm)(dy - dym + dy/2)\, dx\, \rho_2(1 - \alpha_1)$.

For a different direction of the velocity vector O–O′, mass transfer is organized using the same principle.

Thus, the algorithm organizes continuous flow of masses. The calculation stability is affected by the porosity and density of the gas phase, which, in this case, also change continuously and are determined by the mass of the disperse phase in the cell. Thus, in the cell on the left, the porosity is $\alpha_{1(i-1,j)} = (V_{\text{calc}} - M_{(i-1,j)}/\rho_2)V_{\text{calc}}$ and the gas density is $\rho_{1(i-1,j)} = \rho^0_{1(i-1,j)}\alpha_{1(i-1,j)}$.

This method allows one to solve the stability problem of the algorithm, thus decreasing the calculation time, to increase the dimensions of the calculation region, and to take into account collisions of particles with one another and with the boundary surface.

In the next stage of integration, an exhaustive search for all particles by pairs is performed to detect particles that collide. In this case, each particle is a sphere, and their relative positions before and after collision are determined from geometric calculations and the known values of the velocities. The particle radius is calculated from the initial porosity and the cell size of the calculation region: $R = [3V_{\text{calc}}(1 - \alpha_1)/(4\pi)]^{1/3}$.

The initial packing of particles in aggregates is specified using the initial porosity and the results of [7]. In inelastic collision, particles exchange momentum and lose some momentum. The coefficient of loss for collision of a particle of quartz sand with a surface is determined experimentally in [8].

In our numerical studies performed using the given model, the initial and boundary conditions are similar to the conditions for the model of the mechanics of continuous media.

The time step was selected for each calculation cycle from the condition $\Delta t = \min[\text{Ku}\, dy/(a_1 + |u_1|)]$, where a_1 is the velocity of sound in the gas: $a_1 = [(kP_1)/\rho_1]^{0.5}$, Ku is the stability coefficient (the Courant number). In our studies, Ku = 0.3–0.5.

Figure 5 shows the variation of the parameters in the mathematical modeling of the phenomenon in the stage of operation of the first source. In experiments, the initial gas pressure in the charge was $P_z = 0.5$ MPa, the total energy of the charge with allowance for the degree of expansion [6] was $E_{\text{total}} = 21$ J, the height of the layer was 0.2 m, and the initial porosity was 0.3.

Results of the mathematical modelling show that, at the beginning of operation of the ith source (see Fig. 1) ejection develops symmetrically about the vertical axis of this source. The variation in the gas-pressure fields (Fig. 5a) below the daytime surface level and above it at the real time $t = 1 \cdot 10^{-3}$ sec is shown by isolines. Figure 5a reflects the qualitative difference between perturbation propagation in the pore space of the mass and in the homogeneous atmospheric medium. Some increase in pressure at the bottom of the mass is due to the presence of the impenetrable bottom surface of the transport tray.

Figure 5b shows the variation in the propagation velocity of the perturbation. This figure is similar in appearance to the character of variation of the pressure fields. The highest velocity at this moment is observed in the pore space.

The evolution of the mass presented in Fig. 5c agrees with experimental results of photorecording the process at the transparent wall of a transport tray. This figure shows the moment of deformation of the camouflet cavity toward the daytime surface and the beginning of development of an ejection cavity.

The operation of the $(i + 1)$th source is presented in Fig. 6. In this stage, the phenomenon develops asymmetrically. The curve of gas-pressure variation (Fig. 6a) shows that this parameter manifests itself most

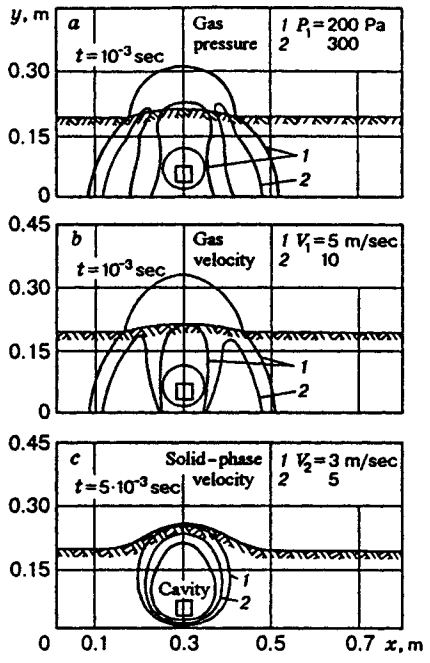

Fig. 5

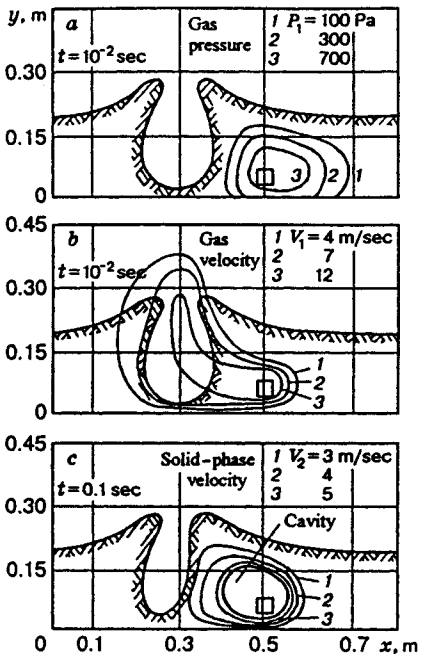

Fig. 6

vividly at the impenetrable bottom surface and in the zone of the mass undisturbed by the first blast. Near the produced camouflet cavity, the pressure is insignificant. This is confirmed by the considerable increase in the gas velocity toward the free space of the opening camouflet cavity (Fig. 6b). The jump in the gas velocity spreads beyond the bottom surface in the zone of the ith ejection.

The velocity of the solid phase is shown by isolines in Fig. 6c, which presents the beginning of displacement of the mass at the bottom surface of the transport tray. It is necessary to note that, at the given moment, the fragments that form the vault of the opening camouflet cavity have a radial velocity relative to the center of the ith source. Therefore, the evolution of fragments to the right of the vertical axis of the ith source is largely determined by collisions of particles. In such interaction, the mass located between the sources acquires a velocity in the direction of transportation, i.e., toward the source that was the first to come into action.

The results of the mathematical modeling show satisfactory agreement with experiments, within 20%.

Thus, the models developed give a detailed illustration of the physical essence of a pin-point blast in a loose material, and they are useful in quantitative analysis of the mechanics of mass transportation. This may find practical use in determining the performance of systems that implement this technology.

In numerical studies of a pin-point physical explosion, the model of the mechanics of continuous media is most suitable for monitoring stresses in a transported material, its packing, filtration processes, and heat exchange in phases. It is appropriate for a description of the process in the camouflet stage of development.

The model of the mechanics of loose media adequately reflects the development of the ejection sheaf in the atmosphere and the evolution of fragments upon their collisions. It is useful for continuous monitoring of the position of discrete masses in space for a description of the process of transportation by production of ejection cavities.

REFERENCES

1. R. I. Nigmatulin, *Foundations of the Mechanics of Heterogeneous Media* [in Russian], Nauka, Moscow (1978).
2. R. I. Nigmatulin, *Dynamics of Multiphase Media*, Part 1, Hemisphere Publ., New York (1991).

3. O. M. Belotserkovskii, *Numerical Simulation in the Mechanics of Continuous Media* [in Russian], Nauka, Moscow (1984).
4. S. Soo, *Fluid Dynamics of Multiphase Systems*, Blaisdell Publ. Corp., Massachusetts–Toronto–London (1967).
5. A. Ban, K. S. Basniev, and V. N. Nikolaev, "On the basic equations of filtration in compressed porous media," *Prikl. Mekh. Tekh. Fiz.*, No. 6, 52–55 (1961).
6. V. V. Borovikov, A. S. Ivanov, and B. A. Pivak, "A pulsed gas-dynamic method of transportation of loose materials," *Fiz. Tekh. Probl. Razrab. Polezn. Iskop.*, No. 3, 44–52 (1995).
7. G. Deresevich, "Mechanics of a granular medium," in: *Problems of Mechanics* [in Russian], Issue 3, Izd. Inostr. Lit., Moscow (1961), pp. 91–152.
8. V. A. Shvab, *On the Main Regularities of the Drag in Horizontal Pipes in Pneumatic Transportation* [in Russian], Izd. Tomsk Univ., Tomsk (1960).